THE JOURNAL OF PHYSICAL CHEMISTRY C

pubs.acs.org/JPCC Article

Color-Tunable Delayed Fluorescence and Efficient Spin−Orbit Charge Transfer Intersystem Crossing in Compact Carbazole-Anthracene-Bodipy Triads Employing the Sequential Electron Transfer Approach

Zafar Mahmood, Maria Taddei, Noreen Rehmat, Laura Bussotti, Sandra Doria, Qinglin Guan, Shaomin Ji,* Jianzhang Zhao,* Mariangela Di Donato,* Yanping Huo, and Yong Heng Xing*

Cite This: https://dx.doi.org/10.1021/acs.jpcc.9b11687 Read Online

ACCESS | Metrics & More | Article Recommendations | Supporting Information

ABSTRACT: Spin−orbit charge transfer intersystem crossing (SOCT-ISC) is a promising approach to develop heavy-atom-free triplet photosensitizers. However, designing a strong visible-light harvesting heavy-atom-free triplet photosensitizer with efficient ISC ability in various solvents is still challenging. Most of the SOCT-ISC triplet photosensitizers exhibit efficient ISC only in solvent of particular polarity. To address this challenge, herein, two triads (**BDP-AN-C-CZ** and **BDP-AN-N-CZ**), composed of carbazole (CZ), anthracene (AN), and bodipy (BDP) moieties, were devised. In these triads, the distance, relative orientation, and position of CZ with respect to the AN moiety were varied to study its effect on photophysical properties, especially on SOCT-ISC efficiency. Electrochemical studies, steady-state, and time-resolved spectroscopies confirmed a sequential photoinduced electron transfer (PET) process in the triads. The fluorescence of the BDP moiety is quenched and a red-shifted CT emission band is observed in the triads, due to the enhanced PET effect, compared to the reference **BDP-AN** dyad. We observed that the SOCT-ISC yield can be enhanced taking advantage of sequential electron transfer. The triad **BDP-AN-C-CZ**, in which the CZ moiety was directly linked to the AN moiety, shows an efficient ISC ability both in low-polarity and high-polarity solvents, and unity triplet quantum yield (Φ_T) was observed in dichloromethane. Femtosecond transient absorption spectroscopy confirmed the fast charge separation process (1.8 ps) in **BDP-AN-C-CZ** as compared to the other triad **BDP-AN-N-CZ** (4.8 ps) and the reference **BDP-AN** dyad (7.7 ps). The triads were used as triplet photosensitizers for triplet−triplet annihilation (TTA) upconversion, and high upconversion quantum yield (Φ_{UC} = 18%) was observed. Interestingly, long-lived (τ_{DF} = 118 μs) and solvent-dependent color-tunable TTA delayed fluorescence was observed in the case of **BDP-AN-C-CZ**.

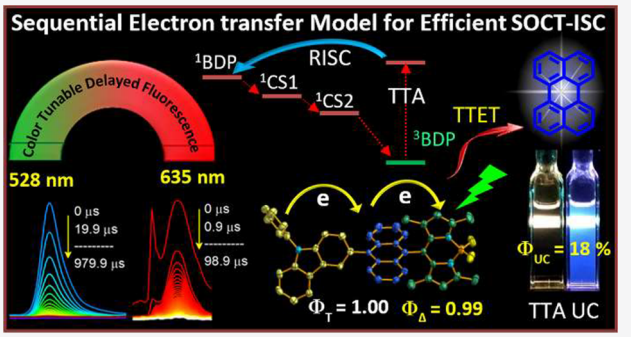

1. INTRODUCTION

Tuning the excited-state properties of organic compounds (triplet photosensitizers, PSs) is essential for designing novel organic materials for applications such as photovoltaics,[1−3] photodynamic therapy,[4−10] luminescence bioimaging,[11,12] artificial photosynthesis,[13] and triplet−triplet annihilation upconversion (TTA).[14−21] The excited-state properties of organic compounds can be tuned either by extending the π-conjugation framework or by attaching the electron-donating/withdrawing substituents.[22,23] In molecular systems having weak to moderate electronic coupling between the donor and acceptor, the intersystem crossing (ISC) properties can be tuned through charge recombination (CR) in the case of electron donor−acceptor systems or hyperfine coupling interaction.[24−28]

The formation of triplet states is essential for a triplet PS. Different strategies have been used to tune the ISC ability of organic chromophores such as heavy-atom effects (I, Br, Pt, Ir, or Ru),[29−35] n−π ↔ π−π* transition (El-Sayed rule),[36] exciton coupling effect,[37−39] and the use of an electron spin convertor.[40−43] All these methods suffer from some drawbacks, for instance, the dark toxicity of heavy atoms and high cost of metals,[44,45] which limit their applications. Other alternative approaches including symmetry breaking charge transfer,[46,47] radical enhanced intersystem crossing,[48,49] and radical pair intersystem crossing (RP-ISC),[50,51] but the required molecular structures are usually synthetically demanding. For instance,

Received: December 18, 2019
Revised: February 9, 2020
Published: February 18, 2020

Scheme 1. Synthesis of Anthracene-Bodipy Derivatives[a]

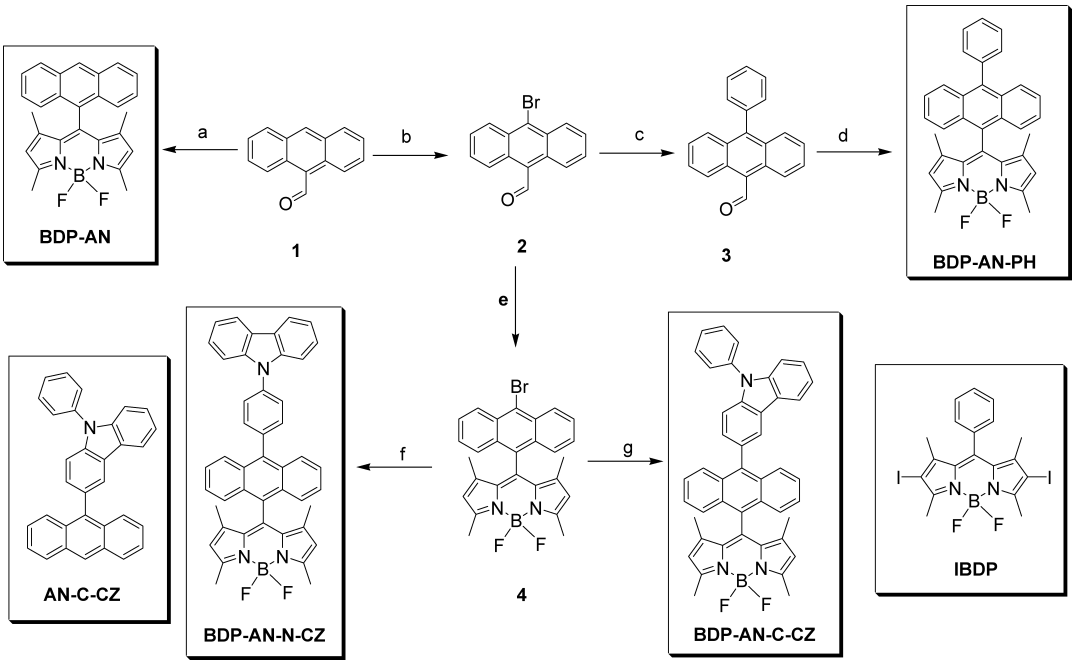

[a]Key: (a) 2−4 Dimethylpyrrole, trifluoroacetic acid, DDQ, stirring for 4 h under N_2, BF_3Et_2O, TEA, yield: 25%. (b) Br_2, $CHCl_3$, RT, overnight, yield: 70%. (c) Phenylboronic acid, K_2CO_3, $Pd(PPh_3)_4$, toluene/EtOH/H_2O, reflux for 8 h, yield: 90%. (d) The reaction conditions are similar to those in panel (a), yield: 25%. (e) The reaction conditions are similar to those in panel (a), yield: 26%. (f) 4-(9*H*-Carbozol-9-yl)phenylboronic acid, K_2CO_3, $Pd(PPh_3)_4$, toluene/EtOH/ H_2O, reflux for 8 h, yield: 77%. (g) 9-Phenyl-9*H*-carbazol-3-ylboronic acid, K_2CO_3, $Pd(PPh_3)_4$, toluene/EtOH/H_2O, reflux for 8 h, yield: 86%.

RP-ISC requires weak coupling between the donor and acceptor, which can only be achieved by connecting them through long non-π-conjugated spacers.[50] In these systems, charge separation (CS) occurs upon photoexcitation, resulting in radical cation and anion pair formation followed by a population of a charge transfer triplet state (^{3}CT) due to hyperfine coupling interaction. The ^{3}CT decays to the lower-lying locally excited triplet state (^{3}LE), which makes the triplet-state formation in such systems not very efficient and long-lived.[52−54]

Recently, a new promising approach for producing triplet states via CR with high quantum yield (QY) has gained much attention due to its various advantages over the conventional RP-ISC. This mechanism, termed spin−orbit charge transfer intersystem crossing (SOCT-ISC), can take place in compact donor−acceptor systems where the electron donor and acceptor are directly linked together without any spacer and assume an orthogonal geometry, thus presenting a rather strong electronic coupling.[25,55−58] As the donor and acceptor are perpendicular to each other, the electron transfer and subsequent charge recombination processes will cause an orbital angular momentum change that compensates the spin flipping angular momentum change associated with ISC, thus resulting in efficient triplet-state formation.[57] The SOCT-ISC is a fast process, usually occurring on the picosecond timescale, whereas RP-ISC is a relatively slow process, taking place on the nanosecond timescale. Recently, a few examples of SOCT-ISC systems based on julolidine-anthracene,[57] phenothiazine-bodipy,[59] phenothiazine-anthracene,[60] naphthyl-acridine,[56] and anthracene-bodipy dyads have been studied.[61,62] Most of these studies are based on simple donor−acceptor molecular design involving direct electron transfer in a single step from the donor to the acceptor moiety. The analysis of SOCT-ISC efficiency in systems involving a multistep or sequential electron transfer process is still mostly unexplored.

Inspired by previous reports, herein, we investigate the possibility to enhance the yield of triplet formation through SOCT-ISC in compact electron donor−acceptor systems involving sequential electron transfer processes. For this study, we designed two new triads by selecting donor and acceptor moieties of appropriate electronic strength and linked in a series (D−D−A) to facilitate sequential electron transfer. The newly synthesized compounds based on carbazole (CZ), anthracene (AN) and bodipy (BDP) chromophores have been characterized using different static and time-resolved spectroscopic techniques, demonstrating that careful modulation of the electronic coupling, exerted through different geometrical constrains in the triads, can effectively produce a notable enhancement of triplet formation. Interestingly, we found satisfactory enhancement in SOCT-ISC yield in triads as compared to the previously reported BDP-AN donor−acceptor system.[61] To the best of our knowledge, this is the first attempt to enhance the triplet yield formation through SOCT-ISC using the sequential electron transfer approach (Scheme 1).

2. EXPERIMENTAL SECTION

2.1. General Methods. All chemicals used in the synthesis of compounds were analytical grade and used as received. UV−vis absorption spectra were measured on a UV-2550 UV−vis spectrophotometer (Shimadzu Ltd., Japan). Fluorescence spectra were obtained on an RF-5301PC spectrofluorometer (Shimadzu Ltd., Japan). Fluorescence quantum yields of the compounds were measured using BDP as a standard (Φ_F = 72% in tetrahydrofuran (THF)).

https://dx.doi.org/10.1021/acs.jpcc.9b11687
J. Phys. Chem. C XXXX, XXX, XXX−XXX

2.2. Synthesis of Compounds. The details of the synthesis and characterization of compounds **2**, **3**, **4**, **BDP-AN**, **BDP-AN-PH**, and **AN-C-CZ** are given in the Supporting Information.

2.3. Synthesis of the Compound BDP-AN-C-CZ. Under a N_2 atmosphere, compound **4** (80 mg, 0.16 mmol), 9-phenyl-9*H*-carbazol-3-ylboronic acid (92 mg, 0.32 mmol), and K_2CO_3 (100 mg, 0.72 mmol) were dissolved in 25 mL of a mixture of $PhCH_3$/EtOH/H_2O (4/2/1, v/v). Then $Pd(PPh_3)_4$ (20 mg, 5 mol %) was added after complete deoxygenation of the above reaction mixture with N_2 bubbling for 20 min. The reaction mixture was allowed to reflux for 8 h under a nitrogen atmosphere. After completion of reaction, the reaction mixture was cooled to room temperature, extracted with CH_2Cl_2 (30 mL), washed with water (2 × 100 mL), and dried over anhydrous sodium sulfate. After evaporation of the solvent under reduced pressure, the crude product was purified with column chromatography (silica gel, CH_2Cl_2/petroleum ether, 2/1, v/v) to give an orange solid (90 mg, yield: 86%). ^{1}H NMR ($CDCl_3$, 400 MHz); δ 8.23 (s, 1H), 8.14 (d, 1H, J = 8.0 Hz), 7.99 (d, 2H, J = 8.0 Hz), 7.80 (d, 2H, J = 12.0 Hz), 7.73−7.62 (m, 5H), 7.55−7.40 (m, 6H), 7.36−7.29 (m, 3H), 5.97 (s, 1H), 5.94 (s, 1H), 2.65 (d, 6H, J = 4.0 Hz), 0.85 (s, 3H), 0.78 (s, 3H). ^{13}C NMR (100 MHz, $CDCl_3$); δ 155.8, 143.0, 141.4, 140.4, 140.2, 139.5, 137.6, 132.5, 130.6, 130.0, 129.7, 129.4, 129.2, 127.9, 127.7, 127.4, 127.2, 126.6, 126.3, 125.5, 125.2, 123.5, 123.1, 121.2, 120.5, 120.2, 110.0, 109.6, 14.7, 13.5, 13.4. MALDI-HRMS ($[C_{45}H_{34}BF_2N_3]^-$) Calcd: m/z = 665.2814. Found: m/z = 665.2809.

2.4. Synthesis of the Compound BDP-AN-N-CZ. **BDP-AN-N-CZ** was prepared using compound **4** (80 mg, 0.16 mmol) and (4-(9-carbazolyl)benzeneboronic acid (92 mg, 0.32 mmol), following a similar method to the synthesis of compound **BDP-AN-C-CZ**. A red solid product was obtained (80 mg, yield: 77%). ^{1}H NMR ($CDCl_3$, 400 MHz); δ 8.22 (d, 2H, J = 8.0 Hz), 8.03−8.01 (m, 2H), 7.86−7.83 (m, 4H), 7.73 (d, 2H, J = 8.0 Hz), 7.67 (d, 2H, J = 8.0 Hz), 7.54−7.46 (m, 6H), 7.38−7.35 (m, 2H), 5.95 (s, 2H), 2.66 (s, 6H), 0.78 (s, 6H). ^{13}C NMR (100 MHz, $CDCl_3$); δ 155.9, 142.9, 140.8, 139.1, 138.2, 137.4, 132.9, 132.5, 129.9, 129.4, 128.7, 126.9, 126.7, 126.01, 126.0, 125.4, 123.6, 121.3, 120.4, 120.2, 109.8, 14.7, 13.4. MALDI-HRMS ($[C_{45}H_{34}BF_2N_3]^-$) Calcd: m/z = 665.2814. Found: m/z = 665.2824.

2.5. X-ray Diffraction Analysis of Single Crystals. Single crystals of the compounds were obtained by slow evaporation of saturated solution in a chloroform−dichloromethane (DCM) mixture solvent at RT. Good quality crystals with appropriate dimensions were used for X-ray analysis. Crystallographic data obtained from X-ray analysis are presented in the Supporting Information. All the measurements were performed on a Burker AXS SMART APEX II CCD spectrometer with a graphite-monochromatized Mo Kα (λ = 0.71073 Å) radiation source. Analysis was performed at RT, and data were acquired using SMART and SAINT programs. The positions of non-hydrogen atoms were found after successful refinement by full-matrix least-squares using the SHELXL-2017 software. The hydrogen atoms of organic frameworks were geometrically fixed at calculated positions and refined by using a riding model. CCDC 1959135 (for **BDP-AN-C-CZ**), CCDC 1959136 (for **BDP-AN-N-CZ**), and CCDC 1959137 (for **BDP-AN**) contains the supplementary crystallographic data for this paper. These data can be obtained free of charge from The Cambridge Crystallographic Data Center via https://www.ccdc.cam.ac.uk.

2.6. Nanosecond Transient Absorption Spectroscopy. The nanosecond transient absorption spectra were acquired on an LP980 laser flash photolysis spectrometer (Edinburgh Instruments, U.K.). The signal was digitized with a Tektronix TDS 3012B oscilloscope. TTA delayed fluorescence of the compounds was also measured on an LP980 laser flash photolysis spectrometer using emission mode, excited with an OpoletteTM 355II + UV nanosecond pulsed laser (OPOTEK, USA). The wavelength was tunable in the range of 210−2200 nm. The samples were deaerated with N_2 for 15 min prior to investigations. The data were processed by LP900 software.

2.7. Femtosecond Transient Absorption Spectroscopy. The transient absorption measurements were carried out using an apparatus based on a Ti:sapphire regenerative amplifier (BMI Alpha 1000) system pumped by a Ti:sapphire oscillator (Spectra Physical Tsunami). The system produces 100 fs pulses at 785 nm, with 1 kHz repetition rate and 450−500 mW average power. Excitation pulses at 400 and 500 nm were obtained by second harmonic generation of the fundamental laser output or by pumping a homemade noncollinear optical paramagnetic amplifier (NOPA) by a portion of the fundamental 785 nm, respectively. The pump beam polarization was set to the magic angle with respect to the probe beam by rotating a $\lambda/2$ plate. The probe pulses were generated by focusing a small portion of the fundamental laser output radiation on a 2 mm thick sapphire window. Pump-probe delays were introduced by sending the probe beam through a motorized stage. Multichannel detection was achieved by sending the white-light continuum after passing through the sample to a flat field monochromator coupled to a homemade CCD detector. TAS measurements were carried out in a quartz cell (2 mm thick) mounted on a movable stage to avoid sample photodegradation and multiple-photon excitation. The recorded kinetic traces and transient spectra were analyzed by using a global-analysis procedure.[77] The number of kinetic components was estimated by performing a preliminary singular values decomposition (SVD) analysis.[78] Global analysis was performed using the GLOTARAN package (http://glotaran.org),[79] employing a linear unidirectional ("sequential") model.

2.8. Theoretical Computations. The ground-state geometries and spin densities of the compounds were optimized using density functional theory (DFT) with the B3LYP functional and 6-31G (d) basis set. Time-dependent DFT (TDDFT) at the B3LYP/6-31G(d) basis set was performed to estimate the excited-state energy and energy gaps between the S_0 state and the triplet excited states of the compounds based on ground-state geometries. All the calculations were performed on Gaussian 09W.

3. RESULTS AND DISCUSSION

3.1. Design and Synthesis of the Compounds. The two triads **BDP-AN-C-CZ** and **BDP-AN-N-CZ** were devised with the aim to enhance the SOCT-ISC by taking advantage of sequential electron transfer. Although the **BDP-AN** donor−acceptor system has been extensively studied, most of the previous reports are based on simple molecular design involving a one-step electron transfer process.[62] Furthermore, these donor−acceptor systems exhibit SOCT-ISC only in polar solvents, whereas no triplet generation was observed in nonpolar solvents. In order to improve the ISC capabilities

https://dx.doi.org/10.1021/acs.jpcc.9b11687
J. Phys. Chem. C XXXX, XXX, XXX−XXX

of these systems, two new triads were synthesized by linking a stronger donor moiety (CZ, HOMO energy level: −5.33 eV vs a HOMO energy level of −5.23 eV for anthryl) to the **BDP-AN** dyad from two different positions, that is, the N-position using a phenyl spacer and the C-position without any spacer. Due to the different geometric constraints, we expect different molecular conformations in two triads leading to different photophysical properties. Considering the donor−acceptor properties of the employed dyes, we expect the occurrence of sequential electron transfer in the triads, with an initial electron transfer from the AN to the BDP moiety followed by a secondary electron transfer from the CZ to the AN moiety.

3.2. X-ray Crystallography. The molecular structures of the triads and the reference **BDP-AN** dyad were confirmed by single-crystal X-ray diffraction analysis (Figure 1). **BDP-AN-C-CZ** crystallized in the triclinic space group *P*-1, $Z = 2$, containing two molecules per unit cell, with a unit cell volume of 3898.1(4) Å^3. Due to the large confirmation restriction of methyl groups at the BDP moiety, the torsion angle between the BDP and AN moieties is 91.3°, nearly orthogonal as anticipated and in agreement with DFT calculations. The centroid-to-centroid distance from AN to BDP is in the range of 4.33−4.36 Å, while the angle between the AN and CZ moieties is in the range of 65.6−70.5° and the bond length between two units is in the range of 7.02−7.05 Å.

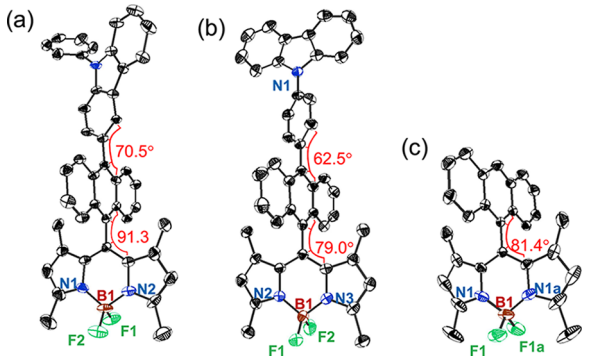

Figure 1. ORTEP view of single-crystal structures of (a) **BDP-AN-C-CZ**, (b) **BDP-AN-N-CZ**, and (c) **BDP-AN** with thermal ellipsoids. Hydrogen atoms and solvent molecules are omitted for clarity.

For **BDP-AN-N-CZ**, the crystal system and space group are triclinic and *P*-1, $Z = 2$, respectively, containing one molecule per unit cell. It was observed that, in **BDP-AN-N-CZ**, BDP and AN moieties also take a nearly orthogonal conformation. The torsion angle and distance between the two units are 79.0° and 4.35 Å, respectively. The angle between the CZ and AN is found to be 76.9°, showing slight deviation from DFT results.

BDP-AN crystallized as the monoclinic crystal in the space group *C*2/*c*, $Z = 4$, containing one molecule per unit cell. The torsion and distance between the two moieties (AN and BDP) are 81.4° and 4.30 Å, respectively. Similar results were obtained with DFT calculations. Significantly, each fluoride atom in the **BDP-AN** molecule is engaged in intermolecular hydrogen bonding (B−F···H) with the π-conjugation system of an anthracene of the neighbor molecule, forming a 2D porous layer, which can be beneficial for the adsorption of specific gases. This topic is out of scope of this paper and will be investigated in future work. The B−F···H bond distance is 2.47 Å (Figure 2).

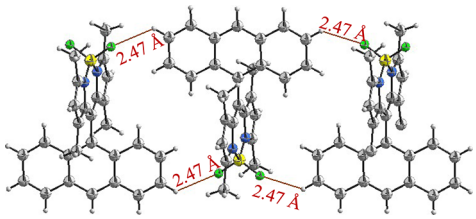

Figure 2. Part of the crystal structure of the compound **BDP-AN**, showing hydrogen bonding using the standard ("ball-and-stick") model.

3.3. UV−vis Absorption and Fluorescence Emission Spectra. The absorption spectra of the triads along with reference compounds were studied (Figure 3a). The absorption spectra of the triads (**BDP-AN-C-CZ** and **BDP-AN-N-CZ**) resemble that of the reference **BDP-AN** dyad and consist of the sum of the absorption profiles of their independent components, and no CT absorption band was observed.[62] This result indicates that there is weak electronic coupling between the donor and acceptor moieties at the ground state.[57,63] Negligible ground-state interaction is reasonable as donor (AN) and acceptor (BDP) moieties are orthogonal to each other, which inhibits π-conjugation.

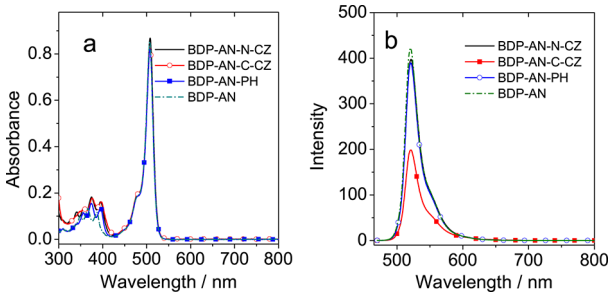

Figure 3. (a) UV−vis absorption spectra of the compounds in toluene, $c = 1.0 \times 10^{-5}$ M. (b) Fluorescence emission spectra of the compounds in toluene, $\lambda_{ex} = 465$ nm, absorbance of the samples at excitation wavelength $A = 0.11$. Optically matched solutions were used (each compound has the same absorbance at the excitation wavelength), 20 °C.

The fluorescence emission of the compounds was studied (Figure 3b). All the dyads and triads exhibit only one emission band at ∼520 nm in low-polarity solvent, toluene (TOL), attributed to the locally excited-state (^{1}LE) emission of the BDP moiety. In the **BDP-AN-C-CZ**, in which the CZ is directly attached at the 3-position to the AN moiety, the fluorescence is comparatively quenched as compared to all other derivatives. The fluorescence quantum yield (Φ_F) of **BDP-AN-C-CZ** is 50% in toluene, which is lower than the reference **BDP-AN** dyad ($\Phi_F = 84\%$). This result indicates that electron transfer (PET) is more efficient in **BDP-AN-C-CZ** than in other derivatives, even in low-polarity solvents such as toluene.

The fluorescence emission spectra of the compounds were also studied in polar solvents, such as dichloromethane and acetonitrile (ACN) (Figure 4 and Supporting Information, Figure S21). In dichloromethane, two emission bands were observed in both triads; the band centered at a shorter wavelength, ∼520 nm, is assigned to the ^{1}LE emission of the BDP chromophore, while the emission band at a longer wavelength, around 600 nm, is interpreted as a CT emission

https://dx.doi.org/10.1021/acs.jpcc.9b11687
J. Phys. Chem. C XXXX, XXX, XXX−XXX

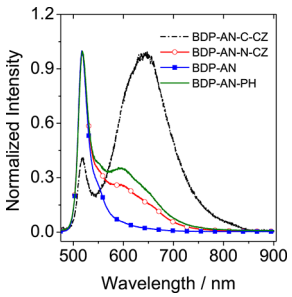

Figure 4. Normalized fluorescence emission spectra of compounds in dichloromethane, λ_{ex} = 465 nm (A = 0.11). Optically matched solutions were used (all the sample solutions have the same absorbance at the excitation wavelength), 20 °C.

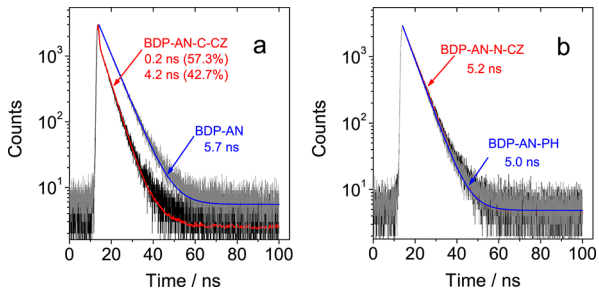

Figure 5. Fluorescence emission decay traces of triads along with their reference compounds: (a) **BDP-AN-C-CZ** and **BDP-AN**, (b) **BDP-AN-N-CZ** and **BDP-AN-PH**, (λ_{ex} = 510 nm), monitored at 520 nm. c = 1.0 × 10^{-5} M in dichloromethane, 20 °C.

band since it is structureless and solvent-polarity-dependent.[25,57,64] The comparison of the normalized emission spectra of triads and reference compounds shows that, in **BDP-AN-C-CZ**, the LE emission is more quenched and weaker than CT emission, while the reference compound **BDP-AN** shows only LE emission. Moreover, the CT emission band in **BDP-AN-C-CZ** is more red-shifted (645 nm) and strong as compared to other derivatives (595 nm). These results are a further indication of strong PET occurring in **BDP-AN-C-CZ**.

The **BDP-AN-N-CZ** triad instead exhibits similar spectral features to the reference compound **BDP-AN-PH**; namely, in both cases, the LE emission band is stronger than the CT emission band. This implies that the CZ moiety has weak excited-state electronic interaction in **BDP-AN-N-CZ** because it is linked to the AN moiety through a phenyl spacer. The fluorescence transition dipole moment (^{1}CT → S_0) and the electronic coupling matrix at the CSS were calculated using eqs 1 and 2 and are reported in Table 1.[54,65] It was found that the

Table 1. Charge-Transfer-Related Photophysical Parameters of the CT Band, Dipole Moments, and Electronic Coupling Matrix Elements of the Compound

compound	ν_{flu}^{CT}[b] (cm^{-1})	k_r^{CT}[c] (10^6 s^{-1})	K_{nr}^{CT}[d] (10^8 s^{-1})	M_{fl}[e] (D)	V_{DA}[f] (eV)
BDP-AN-C-CZ	15,060	1.74	4.3	0.74	0.07
BDP-AN-N-CZ	15,432	2.73	3.0	0.93	0.09
BDP-AN-PH	15,503	2.86	3.5	0.95	0.08
BDP-AN	15,772	11.2	3.3	1.03	0.10

[a]In acetonitrile. [b]The emission wavenumber of the CT band. [c]The radiative rate constant of CT fluorescence. [d]The nonradiative rate constant. [e]The transition dipole moment of the S_0 ← ^{1}CT transition. [f]The electronic coupling between ground state and CT state.

radiative rate constant and transition dipole moment of **BDP-AN-C-CZ** are lower than those of the other derivatives, which is consistent with the fluorescence emission results.

$$|M_{fl}|^2 = \frac{3hk_r}{64\pi^4(n\tilde{\nu}_{fl})^3} \quad (1)$$

$$V_{DA} = \left[\frac{1.4 \times 10^5 k_r^{CT}}{\eta^3 R_c^2 \nu_{flu}^{CT}}\right]^{1/2} \quad (2)$$

The fluorescence decay curves of the triads along with the reference compounds were measured both at LE and CT emission bands (TCSPC detection method, Figure 5 and Supporting Information, Figure S23). In dichloromethane, the fluorescence of **BDP-AN-C-CZ** decays following a biexponential kinetics, with a fast decay component (τ_1 = 0.2 ns, population ratio: 57.3%) and a slow component (τ_2 = 4.2 ns, population ratio: 42.7%), while in all other derivatives, the fluorescence decays with monoexponential kinetics. The fluorescence lifetime of **BDP-AN-C-CZ** (3.3 ns) is much shorter than that of the reference **BDP-AN** dyad (5.6 ns). This quenched fluorescence lifetime in the **BDP-AN-C-CZ** triad is assigned to an enhanced PET effect.[66,67] On the other hand, **BDP-AN-N-CZ** exhibits a fluorescence lifetime (5.2 ns) similar to the reference dyad **BDP-AN-PH** (5.0 ns). The enhanced PET in the **BDP-AN-C-CZ** triad as compared to the **BDP-AN** dyad can be due to sequential electron transfer in the triad. The fluorescence lifetimes of the compounds were also studied in other solvents (Table 2 and Supporting Information, Figures S22 and S23). It was observed that, in polar solvents, the LE fluorescence of the triads decays faster than that in nonpolar solvents, which is in agreement with the fluorescence emission study.

The detailed photophysical properties of the compounds are summarized in Table 2. The **BDP-AN-C-CZ** triad exhibits red-shifted CT emission and low fluorescence quantum yield as compared to the other derivatives, which is in agreement with its enhanced PET. Due to the efficient PET in **BDP-AN-C-CZ**, it is assumed that the charge separated state (CSS) becomes lower in energy (confirmed in later section), thus enabling efficient triplet population through CR, both in polar and nonpolar solvents. To verify this assumption and confirm the ISC ability of the compounds, singlet oxygen ($^1O_2$) quantum yields (Φ_Δ) were measured in different solvents (Table 3). For **BDP-AN-C-CZ**, efficient $^1O_2$ generation was observed in the low-polarity solvent toluene (Φ_Δ = 0.48), and unity $^1O_2$ quantum yield (Φ_Δ = 1.0) was observed in dichloromethane. However, in the case of other derivatives, negligible singlet oxygen generation was observed in toluene. Furthermore, all the derivatives show solvent-polarity-dependent $^1O_2$ production, which supports the SOCT-ISC mechanism. The triplet quantum yield (Φ_T) of the compounds in different solvents was also calculated using the ground-state depletion method (Table 3).

3.4. Electrochemical Study. In order to study the feasibility of electron transfer and to determine the energy levels of CSS of the compounds, electrochemical measurements were carried out (Figure 6). For careful analysis and proper assigning of oxidation and reduction wave potentials in triads, the electrochemical properties of the reference dyads were also studied.

https://dx.doi.org/10.1021/acs.jpcc.9b11687
J. Phys. Chem. C XXXX, XXX, XXX−XXX

Table 2. Photophysical Parameters of Triads and Reference Compounds

compound	solvent	λ_{abs} [a]	ε [b]	λ_{em}	Φ_F [c]	τ_F [d] (ns)
BDP-AN-N-CZ	TOL	508/375	8.7/1.8	521	0.84	6.1
	THF	505/373	8.2/1.8	518	0.30	6.2
	DCM	505/374	8.0/1.9	518/600	0.01/0.02	5.2
	ACN	502/372	7.6/1.9	514/648	0.001/0.009	2.1[e]/3.3[f]
BDP-AN-C-CZ	TOL	507/376	8.3/1.8	521	0.50	6.8
	THF	504/375	7.8/1.8	516/600	0.05	4.7
	DCM	505/375	7.7/1.8	519/643	0.006/0.01	3.3/3.9
	ACN	502/374	7.2/1.8	513/664	0.0006/0.004	0.5[e]/2.3[f]
BDP-AN-PH	TOL	508/375	8.2/1.6	521	0.78	6.0
	THF	505/373	8.0/1.6	517	0.28	6.2
	DCM	505/374	8.0/1.6	518/599	0.01/0.02	5.0[e]/5.1[f]
	ACN	502/372	7.5/1.6	514/645	0.002/0.008	4.0[e]/2.8[f]
BDP-AN	TOL	507/366	8.5/1.4	521	0.83	5.8
	THF	505/366	8.4/1.3	516	0.69	6.0
	DCM	505/366	8.3/1.4	517	0.14	5.6
	ACN	502/365	7.9/1.4	509/634	0.01/0.01	4.8[e]/3.0[f]
AN-C-CZ	TOL	368	1.2	418	0.75	3.7
	ACN[g]			437	0.46	3.6

[a]In different solvents (1.0×10^{-5} M). The wavelength is in nm. [b]Molar absorption coefficient (10^4 M^{-1} cm^{-1}). [c]Fluorescence quantum yield, BDP as standard (Φ_F = 0.72 in THF). [d]Luminescence lifetimes, λ_{ex} = 510 nm (EPL picosecond pulsed laser). [e]At shorter wavelength. [f]At longer wavelength. [g]λ_{abs} and ε were not measured.

For **BDP-AN**, one reversible reduction wave at −1.67 V and one reversible oxidation wave at +0.78 V were recorded, which is assigned to the BDP moiety (Figure 6, Table 4). One irreversible oxidation wave at +1.06 V was also observed, which belongs to the AN moiety. In the case of the other reference dyad **AN-C-CZ**, two irreversible oxidation waves at +0.63 and +0.93 V were observed, which can be assigned to CZ and AN, respectively. The cyclic voltammogram of **BDP-AN-C-CZ** exhibits one reduction wave at −1.67 V, similar to that of the reference **BDP-AN** dyad and belongs to the BDP moiety. One

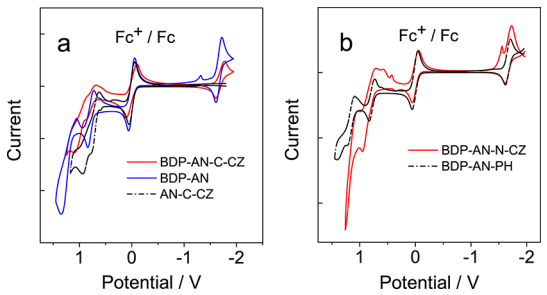

Figure 6. Cyclic voltammogram of the compounds: (a) **BDP-AN-C-CZ**, **BDP-AN**, and **AN-C-CZ**; (b) **BDP-AN-N-CZ** and **BDP-AN-PH**. In deaerated dichloromethane containing 0.10 M Bu_4NPF_6 as the supporting electrolyte, ferrocene (Fc) was used as the internal reference. Scan rates: 50 mV/s. $c = 1 \times 10^{-3}$ M, 20 °C.

Table 4. Electrochemical Redox Potentials of the Compounds[a]

compounds	E(ox) (V)	E(red) (V)
BDP-AN-C-CZ	+0.56, +0.77, +0.97	−1.67
BDP-AN-N-CZ	+0.58, +0.82, +1.04	−1.66
BDP-AN	+0.78, +1.06	−1.67
BDP-AN-PH	+0.78, +1.07, +1.20	−1.66
AN-C-CZ[b]	+0.63, +0.93	

[a]Cyclic voltammetry in N_2-saturated DCM containing a 0.10 M Bu_4NPF_6. The counter electrode is the Pt electrode, the working electrode is the glassy carbon electrode, and the $Ag/AgNO_3$ couple is the reference electrolyte. [b]E(red) was not observed.

irreversible oxidation wave at +0.56 V and two reversible oxidation waves at +0.77 and +0.97 V were also recorded, which belong to CZ, BDP, and AN moieties, respectively. Similarly, **BDP-AN-N-CZ** shows one reduction wave at −1.66 V and three oxidation waves at +0.58, +0.82, and +1.04 V, respectively.

The thermodynamic feasibility values for PET between donor units (AN and/or CZ) and acceptor unit (BDP) in dyads and triads were calculated using the Rehm−Weller equation (see the Supporting Information for details).[68,69] The free energy changes of electron transfer in dyads and triads from AN to BDP upon excitation of BDP are listed in Table 5. In the case of **BDP-AN**, a 0.08 eV ΔG^0_{CS} value was observed for PET from the AN unit to the BDP moiety in toluene, which indicates that PET is not a favorable process in low-polarity solvents. For **BDP-AN-C-CZ**, favorable ΔG^0_{CS} values of −0.006 and −0.26 eV for PET in toluene from AN to BDP and from CZ to BDP moieties were observed, respectively, which indicates that PET is a thermodynamically allowed process in the **BDP-AN-C-CZ** triad even in low-polarity

Table 3. Triplet Excited State Kinetic Parameters of Compounds

	BDP-AN-N-CZ			BDP-AN-C-CZ			BDP-AN-PH			BDP-AN		
solvent	τ_T [a]	Φ_T [b]	Φ_Δ [c]	τ_T [a]	Φ_T [b]	Φ_Δ [c]	τ_T [a]	Φ_T [b]	Φ_Δ [c]	τ_T [a]	Φ_T [b]	Φ_Δ [c]
TOL	248	0.04	0.07	197	0.46	0.48	291	0.06	0.08	314	0.03	0.04
THF	–[d]	–[d]	0.42	–[d]	–[d]	0.53	–[d]	–[d]	0.40	–[d]	–[d]	0.24
DCM	95	0.90	0.94	98	1.00	0.99	98	0.90	0.91	87	0.86	0.84
ACN	67	0.99	0.91	75	0.80	0.72	83	0.92	0.88	64	0.90	0.86

[a]Triplet-state lifetime, measured by a nanosecond transient absorption spectrometer in deaerated solvents (1.0×10^{-5} M) and in μs. [b]Triplet quantum yield measured by the ground-state depletion method using 2,6-diodobodipy as standard (Φ_T = 0.88 in toluene). [c]Singlet oxygen quantum yield measured with 2,6-diiodobodipy as standard (Φ_Δ = 0.87 in DCM). [d]Not measured.

https://dx.doi.org/10.1021/acs.jpcc.9b11687
J. Phys. Chem. C XXXX, XXX, XXX−XXX

Table 5. Driving Forces of Charge Recombination (ΔG^0_{CR}) and Charge Separation (ΔG^0_{CS}) and the Energy of Charge Separated State (CSS) for Dyads/Triads in Different Solvents[a]

	ΔG^0_{CS} (eV)			ΔG^0_{CR} (eV)			E_{CSS} (eV)		
compound	TOL	DCM	ACN	TOL	DCM	ACN	TOL	DCM	ACN
BDP-AN-C-CZ	−0.006	−0.16	−0.20	−2.42	−2.26	−2.22	2.42	2.26	2.22
BDP-AN-N-CZ	0.05	−0.10	−0.15	−2.48	−2.33	−2.28	2.48	2.33	2.28
BDP-AN	0.08	−0.07	−0.11	−2.51	−2.36	−2.32	2.51	2.36	2.32
BDP-AN-PH	0.07	−0.07	−0.12	−2.50	−2.35	−2.31	2.50	2.35	2.31

[a] E_{00} = 2.43 eV was used for dyads and triads. E_{00} is the approximated energy level with the cross point of UV−vis absorption and fluorescence emission after normalization at the singlet excited state.

solvents. These results are in agreement with low Φ_F and high Φ_Δ of **BDP-AN-C-CZ** in toluene as compared to other derivatives.

PET is not favorable for **BDP-AN-N-CZ** in toluene as ΔG^0_{CS} values for PET from AN to BDP and CZ to BDP are 0.05 and 0.15 eV, respectively. We found that the CT-state energy levels decrease in polar solvents (Table 5), and ΔG^0_{CS} values indicate that the CS is thermodynamically allowed for all dyads/triads in polar solvents, which is in agreement with other experimental observations (Table 2). This prediction was also confirmed by the fluorescence quenching of compounds in polar solvents.

3.5. Nanosecond Transient Absorption Study. To study the triplet-state population of the triads, nanosecond transient absorption spectra were measured. All the derivatives show identical transient absorption profiles (Figure 7 and

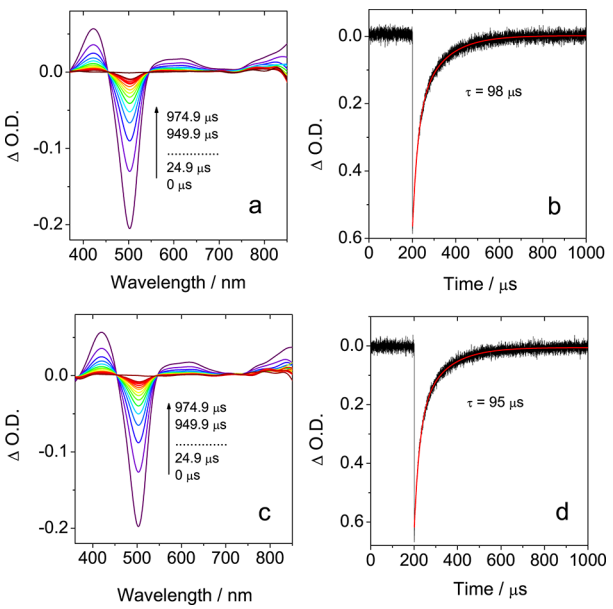

Figure 7. Nanosecond transient absorption spectra of compounds: (a) **BDP-AN-C-CZ** and (c) **BDP-AN**, upon ns pulsed laser excitation (λ_{ex} = 502 nm). Panels (b) and (d) are their respective decay curves at 505 nm, c = 1.0 × 10^{-5} M in dichloromethane, 20 °C.

Supporting Information, Figures S25−S29). Upon photoexcitation at 502 nm, the ground-state bleaching (GSB) band centered at 500 nm and two excited-state absorption bands (ESA) centered at 420 and 610 nm were observed, similar to that observed for an isolated BDP chromophore. These measurements confirm that ISC occurs in the triads and the triplet state is localized on the BDP chromophore.[32,70] Furthermore, the triplet-state lifetime is comparable in all derivatives, although the quantum yield of triplet formation is strongly enhanced in **BDP-AN-C-CZ** in nonpolar solvents (see Table 3). In the case of **BDP-AN-C-CZ**, a long-lived triplet excited state (248 μs) was observed in toluene, but with increasing solvent polarity, the lifetime becomes shorter (98 μs). Similar results were observed in the other triad and reference dyads (Supporting Information, Figures S25−S29).

3.6. Femtosecond Transient Absorption Study. To verify the occurrence of cascade electron transfer processes in the triads, we measured the transient absorption spectra of the compounds in the 0.1 ps−1.5 ns time interval. The samples were excited at 400 nm, a wavelength which is predominantly exciting the AN moiety. To extract the time constants of the photoinduced processes occurring in the samples, global analysis of the transient absorption data was performed, which consists of fitting simultaneously all the registered kinetic traces with combinations of exponential functions. Using a kinetic scheme based on a sequential decay, the fit allows estimation of the kinetic constants describing the dynamic evolution of the system and the associated spectral components, called evolution associated difference spectra (EADS). Figure 8 reports the EADS obtained by analyzing the

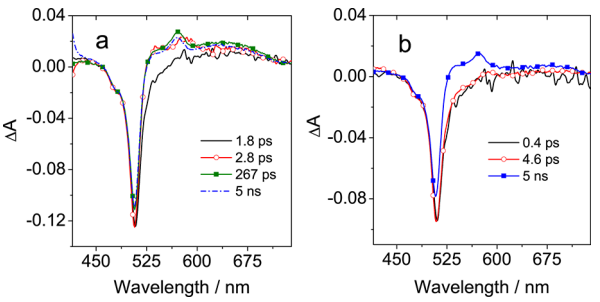

Figure 8. Evolution associated difference spectra obtained from global analysis of time-resolved data measured for (a) **BDP-AN-C-CZ** and (b) **BDP-AN-N-CZ** in DCM. λ_{ex} = 400 nm.

transient absorption data recorded for the two triads **BDP-AN-C-CZ** and **BDP-AN-N-CZ** in dichloromethane. Based on the rationale used in designing the triads, we expect a sequence of events taking place upon excitation of the AN unit. The first envisaged process is energy transfer toward the BDP, populating a local excited (LE) state. From here, electron transfer is expected to take place, initially producing the CZ-$AN^{\bullet+}$-$BDP^{\bullet-}$ radical pair, as already observed in different **BDP-AN** dyads.[25,71] In the following, the hole could be transferred on the CZ moiety, forming $CZ^{\bullet+}$-AN-$BDP^{\bullet-}$.

The initial spectral component obtained by analyzing the transient absorption data for **BDP-AN-C-CZ** (black line, Figure 8a) presents an intense negative band due to the

https://dx.doi.org/10.1021/acs.jpcc.9b11687
J. Phys. Chem. C XXXX, XXX, XXX−XXX

bleaching of the BDP moiety and a broad positive feature extending from 550 to 720 nm. In the previous literature, the absorption band in the 570−590 nm range was assigned to the characteristic signature of BDP anion formation, and the appearance of a band in the 700 nm region was assigned to the formation of the AN cation.[25,71] Although not well resolved at early times, the appearance of the positive feature in the 550 to 720 nm region in the first EADS could indicate initial charge separation, whose dynamics occurs on a timescale similar to that of energy transfer. Upon 1.8 ps, a band centered at 580 nm, which can be assigned to $BDP^{\cdot-}$ (red EADS, Figure 8a), can be clearly observed. At the same time, the signal intensity in the 530−550 nm region increases, going from negative to positive, and a broad band centered at about 640 nm develops. In the following spectral evolution, occurring in about 2.8 ps, the $BDP^{\cdot-}$ band centered at 580 nm blue-shifts by 10 nm and further increases in intensity (evolution from red to green EADS). Finally, on the longer timescale, the overall transient signal slightly decreases in intensity, although a substantial excited-state population remains on the ns timescale, as expected considering the high triplet yield observed for this sample. The evolution is quite similar also in the case of **BDP-AN-N-CZ**, with the only difference that the positive bands are comparatively less intense and that both the change in sign in the 530−550 nm region and the the development of the broad band at 640 nm occur on a slower timescale of 4.8 ps. The previous literature indicated that the CZ cation has an absorption band centered at around 540 nm,[72] which in our sample could be covered due to superposition with the bleaching signal of the BDP. However, the increase in intensity in the 530−550 nm region could well signal the formation of $CZ^{\cdot+}$. Furthermore, since the 640 nm band was not observed in previous measurements executed for a **BDP-AN** dyad (see the Supporting Information, Figure S31), we conclude that this band is also attributable to the carbazole moiety.

In the case of the dyad, where the final CT state is $BDP^{\cdot-}$-$AN^{\cdot+}$, absorption bands at 570 nm due to $BDP^{\cdot-}$ and 720 nm due to $AN^{\cdot+}$ were indeed observed (Figure 9a). Based on these

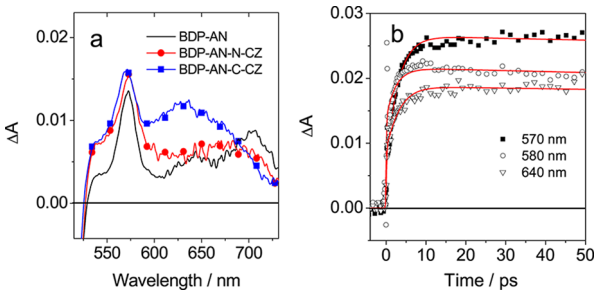

Figure 9. (a) Comparison of the long-lived spectral component for **BDP-AN-C-CZ**, **BDP-AN-N-CZ**, and **BDP-AN**; the signals have been normalized on the BDP bleaching band.(b) Kinetic traces at cation and anion characteristic absorption wavelengths for **BDP-AN-C-CZ** in DCM.

spectral assignments, we identify the 1.8 ps component to be associated with the initial PET in **BDP-AN-C-CZ** and the 2.8 ps component to be due to the formation of the secondary radical pair. The kinetic traces at the maximum of the anion-cation bands are reported in Figure 9b for **BDP-AN-C-CZ**. The band at 640 nm is well visible in the case of **BDP-AN-C-CZ** and less intense for **BDP-AN-N-CZ**. Furthermore, in **BDP-AN-N-CZ**, both the signal inversion in the 530−550 nm region and the rise of the broad absorption at 640 nm occur on a slower timescale of 4.8 ps. We thus conclude that the formation of the secondary radical pair is faster and more efficient for the first dyad, in line with its higher triplet quantum yield.

The introduction of the CZ moiety increases the yield of charge separation also in nonpolar solvents, particularly in the case of **BDP-AN-C-CZ**. Figure 10 shows the EADS obtained

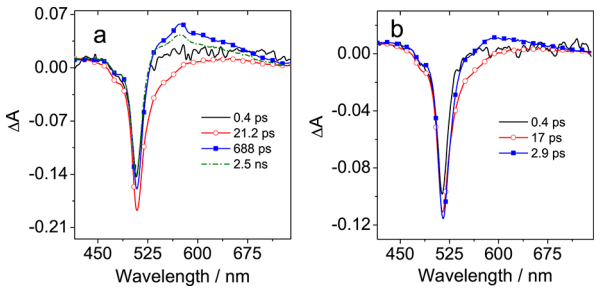

Figure 10. Evolution associated difference spectra obtained from global analysis of time-resolved data measured for (a) **BDP-AN-C-CZ** and (b) **BDP-AN-N-CZ** in toluene. λ_{ex} = 400 nm.

by analyzing the transient absorption data recorded upon 400 nm excitation for **BDP-AN-C-CZ** and **BDP-AN-N-CZ** in toluene. The characteristic $BDP^{\cdot-}$ band is observed to rise for **BDP-AN-C-CZ**, together with a broad band extending up to 700 nm, which we assign to the CZ unit. In the case of **BDP-AN-N-CZ**, charge separation appears less efficient, as evidenced by the comparatively lower intensity of the anion and cation bands. Furthermore, for both triads, the kinetics of photoinduced electron transfer is slower than in dichloro-methane. Indeed, in this case, energy transfer from the AN to the BDP moiety, occurring in about 0.5 ps in both samples (evolution from black to red EADS) and evidenced by the increase of the BDP bleaching signal, can be clearly distinguished from PET. The positive signals due to anion and cation formation increase for both dyads on a timescale of the order of 17−20 ps. Finally, it is worth noticing that, in all cases, direct excitation into the BDP at 500 nm reduces the yield of charge separation, particularly when nonpolar solvents are used (Supporting Information, Figures S40−S43).

3.7. Theoretical Computations. In order to rationalize the photophysical properties, the ground-sate geometries of triads and reference dyads were optimized with the DFT method (Figure 11 and Supporting Information, Figure S48).

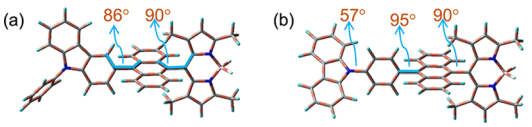

Figure 11. Optimized conformations of ground state and the dihedral angles (degree) of triads: (a) **BDP-AN-C-CZ** and (b) **BDP-AN-N-CZ**. Calculated at the DFT (B3LYP/6-31G (d)) level with Gaussian 09W.

For **BDP-AN-C-CZ**, the AN and BDP moieties take the orthogonal conformation (90°) due to the steric hindrance of methyl groups on the BDP moiety, while the angle between AN and CZ moiety is 87°, which is also nearly orthogonal (Figure 11). These results are in agreement with the single-crystal X-ray structure; only slight deviation in angles was

https://dx.doi.org/10.1021/acs.jpcc.9b11687
J. Phys. Chem. C XXXX, XXX, XXX−XXX

observed. In the case of **BDP-AN-N-CZ**, the angle between BDP and AN was also found to be orthogonal. However, CZ and AN moieties are with 36.8° dihedral angles between the two planes. The non-orthogonal conformation of AN and CZ moieties in **BDP-AN-N-CZ** is due to a minor conformation restriction as there is an intervening phenyl spacer between the two moieties. The angle of the intervening phenyl spacer with the AN moiety is 95°, while the angle between the phenyl and CZ moiety is 57°.

The frontier molecular orbitals show that, in all compounds, the highest occupied molecular orbital (HOMO) is localized on the AN moiety, while the lowest unoccupied molecular orbital (LUMO) is localized on the BDP chromophore (Supporting Information, Figure S48). This result confirms that, in both triads and dyads, AN is more likely to be the electron donor and BDP acts as the acceptor, and there is a possibility of electron transfer in the compounds upon photoexcitation. Moreover, the separation of HOMO and LUMO orbitals and the computed dihedral angles indicate that there is weak electronic interaction at the ground state, which is in agreement with UV−vis absorption spectra of the compounds (Figure 3b).

Furthermore, the frontier molecular orbital study also supports the sequential electron transfer process in **BDP-AN-C-CZ**. The localization of the HOMO on AN and LUMO on the BDP supports the occurrence of the first electron transfer from AN to BDP. The localization of the HOMO−2 orbital on the CZ moiety supports that, at the later stage, the hole migrates toward CZ, in agreement with the experimental study. The separation of HOMO and LUMO orbitals also facilitates the SOCT-ISC process, which is in line with efficient ISC and high triplet yield of triads.

To further support our results, the electron spin density surfaces of the radical anion and radical cation of compounds were also calculated (Figure 12). The spin density distribution

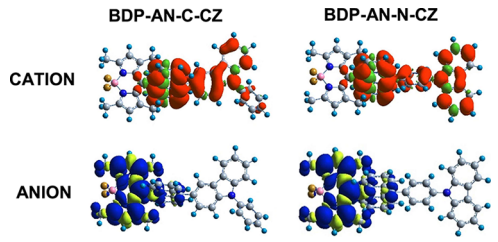

Figure 12. Spin density distribution of the triads, anions (charge = −1) and cations (charge = +1) obtained by computation with DFT theory at the (UB3LYP/6-31G (d)) level using Gaussian 09W.

of radical cations and anions gives the information of the presence of holes and electrons of the CT state. The result shows that, in both triads, the hole is confined equally on the AN and CZ moieties while the electron is localized on the BDP chromophore, which indicates that BDP acts more likely as an acceptor while both AN and CZ act as electron donors in the triads. The equal distribution of holes on AN and CZ indicates that both moieties take part in the PET process, thus supporting the sequential electron transfer process in triads.

In order to study the delocalization of the triplet state of compounds, the spin densities of triads and dyads were calculated (Figure 13). In all compounds, the spin density is localized on the BDP, in agreement with the nanosecond transient absorption study (Figure 7, Supporting Information, Figures S25−S29).

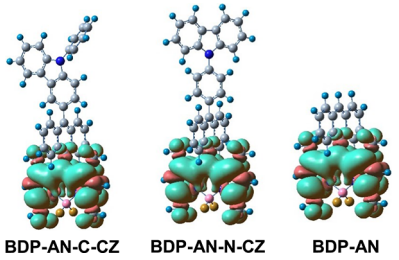

Figure 13. Spin density distribution of the triplet states of the triads and reference dyad obtained by computation with DFT theory at the (B3LYP/6-31G (d)) level using Gaussian 09W.

3.8. Triplet−Triplet Annihilation Upconversion. The strong visible-light absorption and high triplet yield of the devised triads make these compounds ideal triplet photosensitizers. To confirm their potential application, the triads based on CR-induced ISC were utilized in TTA upconversion.

On the basis of the triplet excited-state energy level (T_1) of the triads (1.58 eV), we selected perylene (triplet state energy: 1.53 eV) as the triplet acceptor/emitter for upconversion. By using a suitable concentration of triplet acceptor perylene, the triads showed high upconversion quantum yield (Φ_{UC}) in dichloromethane, upon photoexcitation with a 510 nm pulsed laser. **BDP-AN-C-CZ** shows high Φ_{UC} of 18% in dichloromethane (Figure 14), which is about 2 times that of the **BDP-**

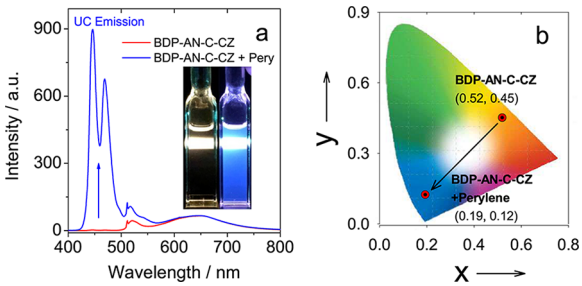

Figure 14. (a) TTA upconversion with **BDP-AN-C-CZ** as the photosensitizer and perylene (Pery) as the acceptor. Excited with a 510 nm cw laser (50 mW cm^{-2}). c[perylene] = 2.0 × 10^{-5} M, in deaerated dichloromethane, 20 °C. Inset: photographs of **BDP-AN-C-CZ** alone and the upconversion. (b) CIE diagram.

AN dyad under the same conditions (dichloromethane, c = 1.0 × 10^{-5} M, and 50 mW cm^{-2} power density).[61] The upconverted emission is visible to the naked eye, and coordinates of the CIE diagram are also in agreement with photographs (Figure 14b). In the case of **BDP-AN-N-CZ**, 15% Φ_{UC} was observed (Supporting Information, Figure S44), while the reference **BDP-AN** dyad shows only 10% Φ_{UC} in dichloromethane. Moreover, **BDP-AN-C-CZ** also shows a 6% Φ_{UC} in toluene, while in the case of the other triad and dyads, no upconversion was observed in toluene (Supporting Information, Figure S46).

3.9. Delayed Fluorescence. Previously, we reported that **BDP-AN** shows delayed fluorescence by using the nanosecond transient absorption spectrometer in the emission mode.[62] Herein, we report for the first time the observation of solvent-dependent color-tunable delayed fluorescence. In toluene, the triad **BDP-AN-C-CZ** shows delayed fluorescence at wave-

https://dx.doi.org/10.1021/acs.jpcc.9b11687
J. Phys. Chem. C XXXX, XXX, XXX−XXX

lengths similar to the **BDP-AN** dyad upon photoexcitation with a ns pulsed laser (1.8 mJ/pulse, pulse duration: 5 ns, Figure 15). Interestingly, long-lived delayed fluorescence was

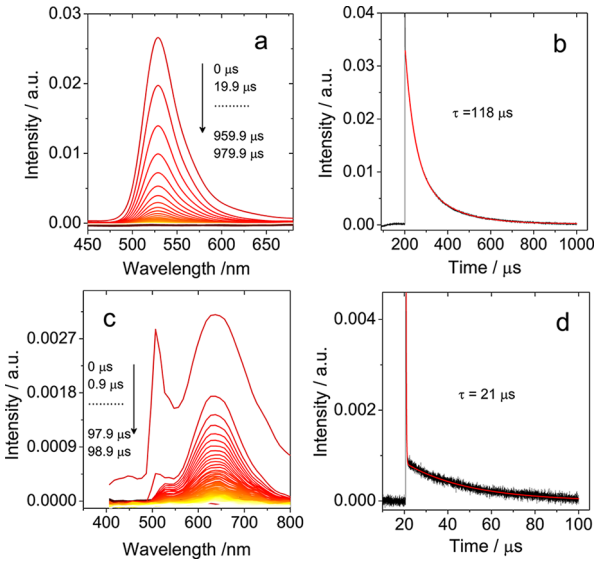

Figure 15. Delayed fluorescence of **BDP-AN-C-CZ** upon nanosecond pulsed laser excitation (λ_{ex} = 505 nm, 1.8 mJ/pulse, pulse duration: 5 ns). (a) Nanosecond transient emission spectra of **BDP-AN-C-CZ** in deaerated toluene. (b) Decay traces at 525 nm in deaerated toluene. (c) Nanosecond transient emission spectra of **BDP-AN-C-CZ** in deaerated dichloromethane. (d) Decay traces at 637 nm in deaerated dichloromethane 20 °C.

observed with triad **BDP-AN-C-CZ** in toluene, with a lifetime of 118 μs, which is 4 times longer than the lifetime of the delayed fluorescence observed with the **BDP-AN** dyad in dichloromethane[62] and about 17,000 times longer than the prompt fluorescence lifetime of **BDP-AN-C-CZ** (6.8 ns). The dyad **BDP-AN** did not show any delayed fluorescence in toluene.

Surprisingly, the triad **BDP-AN-C-CZ** shows a red-shifted delayed fluorescence at wavelengths similar to the charge transfer emission in dichloromethane (Figure 15). This is the first obvious report of solvent-dependent color-tunable delayed fluorescence. These results confirmed that, in dichloromethane, the charge transfer process in triad **BDP-AN-C-CZ** is very efficient. The observation of delayed fluorescence at the LE emission band in the nonpolar solvent and at the CT emission band in polar solvents can be explained considering that the PET process is more efficient in polar solvents, making the CS channel faster than the LE decay. Also, in the case of **BDP-AN-N-CZ**, the long-lived delayed fluorescence (τ_{DF} = 53 μs) was also observed in dichloromethane (Supporting Information, Figure S47).

Two different mechanisms can lead to delayed fluorescence in organic compounds, namely, reverse intersystem crossing $T_1 \rightarrow S_1$ (thermally activated delayed fluorescence, also called E-type delayed fluorescence)[73−75] and TTA (which is also known as P-type delayed fluorescence).[76] The delayed fluorescence observed in the triads is P-type as previously reported for **BDP-AN** dyad because P-type delayed fluorescence is more sensitive to excitation power than E-type delayed fluorescence. In the case of triads, delayed fluorescence was not observed upon excitation with a picosecond pulsed laser (5×10^{-7} mJ/pulse, pulse duration 120 ps), used in fluorescence measurements with TCSPC, but observed upon excitation with a strong nanosecond pulsed laser. From these results, we attribute the long-lived fluorescence observed in the triads to P-type delayed fluorescence that occurred via the TTA upconversion mechanism.

The overall photophysical process involved in the **BDP-AN-C-CZ** triad can be summarized through the Jablonski diagram (Scheme 2). Upon photoexcitation of the triad, its singlet

Scheme 2. Supposed Photophysical Process of BDP-AN-C-Car[a]

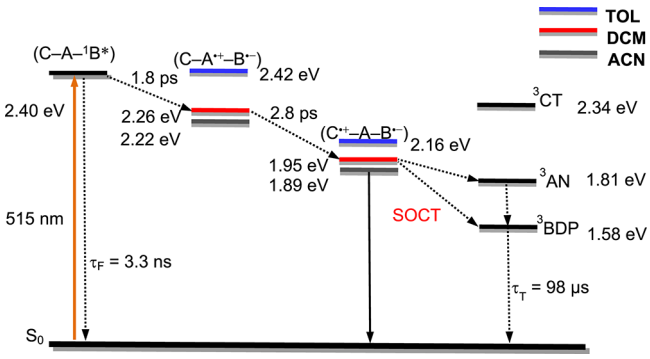

[a]The energy levels of the excited singlet states are derived from the spectroscopic data; the energy level of charge transfer state is obtained from electrochemical data, also confirmed by the CT emission band. The triplet energy levels are estimated by the TD-DFT method. The superscripted numbers indicate the spin multiplicity. C stands for the carbazole unit, A stands for anthracene, and BDP stands for the bodipy unit. The superscripted number designates the spin multiplicity.

excited state is populated, which rapidly evolves to the first CS state through electron transfer from the AN to the BDP chromophore (1.8 ps). Successively, a secondary electron transfer takes place from the electron-rich CZ moiety to the electron-deficient AN moiety forming the second CS state (2.8 ps). On a slower timescale, charge recombination takes place, and the triplet state of BDP chromophore populates. Afterward, delayed fluorescence is produced following the TTA pathway. In the nonpolar solvent, DF is observed at the LE emission band, while in the polar solvent, it is observed at the CT emission band due to the faster PET channel.

In the case of the other triad **BDP-AN-N-CZ**, a similar photophysical process was observed in polar solvents (Supporting Information, Scheme S1), while in the nonpolar solvent toluene, PET is not a thermodynamically feasible process as CSS lies above the singlet excited state, which is in agreement with the fluorescence study (Figure 3b, Table 2). In the dyads, upon photoexcitation, the singlet excited state is populated, which leads to formation of CSS, and afterward, the triplet state is populated following the SOCT-ISC pathway (Supporting Information, Scheme S2).

4. CONCLUSIONS

In summary, we have demonstrated that spin−orbit charge transfer intersystem crossing (SOCT-ISC) efficiency can be improved by utilizing a sequential electron transfer approach. For this study, we devised two new triads (**BDP-AN-C-CZ** and **BDP-AN-N-CZ**) by selecting donor and acceptor moieties of appropriate electronic strength and linked in a series (D−D−A) to facilitate a sequential electron transfer process. The

https://dx.doi.org/10.1021/acs.jpcc.9b11687
J. Phys. Chem. C XXXX, XXX, XXX−XXX

molecular conformation was varied by changing the position of attachment and relative orientation of the carbazole with the anthracene moiety to study its effect on the photophysical properties. The sequential photoinduced electron transfer processes in these triads were confirmed by electrochemical studies, steady-state, and time-resolved spectroscopies. Efficient and fast charge separation (1.8 ps) in **BDP-AN-C-CZ** was revealed by femtosecond transient absorption spectroscopy, while for the reference **BDP-AN** dyad, comparatively slower charge separation (7.7 ps) was observed. The enhanced PET process in **BDP-AN-C-CZ** compared to the reference **BDP-AN** dyad is an indication of sequential electron transfer. These results are consistent with the high triplet yield (Φ_T = 1.0) of **BDP-AN-C-CZ**. Notably, **BDP-AN-C-CZ** exhibits a high singlet oxygen generation ability in solvents of variable polarity (nonpolar to polar), which makes **BDP-AN-C-CZ** a potent triplet photosensitizer and unique from previously reported structure profiles. Long-lived triplet−triplet annihilation (TTA) delayed fluorescence was observed in these triads. Interestingly, we found that TTA delayed fluorescence is dependent on solvent polarity and that color-tunable (green−red, 525−648 nm) delayed fluorescence was observed in **BDP-AN-C-CZ**. Moreover, both triads were used as triplet photosensitizers for the TTA upconversion with perylene as the triplet acceptor/emitter, and high upconversion quantum yield was observed. These studies can be helpful in designing new efficient heavy-atom-free triplet photosensitizers based on the donor−acceptor system. The current research work will also be useful for photovoltaics, photocatalytic organic reactions, artificial photosynthesis, bioimaging, and triplet−triplet annihilation upconversion.

■ ASSOCIATED CONTENT

Supporting Information

The Supporting Information is available free of charge at https://pubs.acs.org/doi/10.1021/acs.jpcc.9b11687.

General experimental methods, ^{1}H NMR, ^{13}C NMR data, and HRMS spectra of the compounds (PDF)

Crystallographic data of **BDP-AN** (PDF)

Crystallographic data of **BDP-AN-C-CZ** (PDF)

Crystallographic data of **BDP-AN-N-CZ** (PDF)

■ AUTHOR INFORMATION

Corresponding Authors

Shaomin Ji − *Light Industry and Chemical Engineering College, Guangdong University of Technology, Guangzhou 510006, P. R. China;* orcid.org/0000-0002-3304-2114; Email: smji@gdut.edu.cn

Jianzhang Zhao − *State Key Laboratory of Fine Chemicals School of Chemical Engineering, Dalian University of Technology, Dalian 116024, P. R. China;* orcid.org/0000-0002-5405-6398; Email: zhaojzh@dlut.edu.cn

Mariangela Di Donato − *ICCOM-CNR, 50019 Sesto Fiorentino (FI), Italy; LENS (European Laboratory for Non-Linear spectroscopy), I-50019 Sesto Fiorentino, Italy;* orcid.org/0000-0002-6596-7031; Email: didonato@lens.unifi.it

Yong Heng Xing − *College of Chemistry and Chemical Engineering, Liaoning Normal University, Dalian 116029, P. R. China;* orcid.org/0000-0002-7550-2262; Email: xingyongheng@lnnu.edu.cn

Authors

Zafar Mahmood − *Light Industry and Chemical Engineering College, Guangdong University of Technology, Guangzhou 510006, P. R. China; State Key Laboratory of Fine Chemicals School of Chemical Engineering, Dalian University of Technology, Dalian 116024, P. R. China*

Maria Taddei − *ICCOM-CNR, 50019 Sesto Fiorentino (FI), Italy*

Noreen Rehmat − *State Key Laboratory of Fine Chemicals School of Chemical Engineering, Dalian University of Technology, Dalian 116024, P. R. China*

Laura Bussotti − *ICCOM-CNR, 50019 Sesto Fiorentino (FI), Italy*

Sandra Doria − *ICCOM-CNR, 50019 Sesto Fiorentino (FI), Italy*

Qinglin Guan − *College of Chemistry and Chemical Engineering, Liaoning Normal University, Dalian 116029, P. R. China*

Yanping Huo − *Light Industry and Chemical Engineering College, Guangdong University of Technology, Guangzhou 510006, P. R. China*

Complete contact information is available at: https://pubs.acs.org/10.1021/acs.jpcc.9b11687

Notes

The authors declare no competing financial interest.

■ ACKNOWLEDGMENTS

We thank the NSFC (21975053, 21975055, 21603021, 21673031, 21761142005, and 21911530095), the Fundamental Research Funds for the Central Universities (DUT2019TA06), State Key Laboratory of Fine Chemicals (ZYTS201901), and Technology Plan of Guangdong Province (2016A010103031) for financial support.

■ REFERENCES

(1) Dai, F.-R.; Zhan, H.-M.; Liu, Q.; Fu, Y.-Y.; Li, J.-H.; Wang, Q.-W.; Xie, Z.; Wang, L.; Yan, F.; Wong, W.-Y. Platinum(II)−Bis(aryleneethynylene) Complexes for Solution-Processible Molecular Bulk Heterojunction Solar Cells. *Chem. − Eur. J.* **2012**, *18*, 1502−1511.

(2) Suzuki, S.; Matsumoto, Y.; Tsubamoto, M.; Sugimura, R.; Kozaki, M.; Kimoto, K.; Iwamura, M.; Nozaki, K.; Senju, N.; Uragami, C.; et al. Photoinduced electron transfer of platinum(II) bipyridine diacetylides linked by triphenylamine- and naphthaleneimide-derivatives and their application to photoelectric conversion systems. *Phys. Chem. Chem. Phys.* **2013**, *15*, 8088−8094.

(3) Congreve, D. N.; Lee, J.; Thompson, N. J.; Hontz, E.; Yost, S. R.; Reusswig, P. D.; Bahlke, M. E.; Reineke, S.; Van Voorhis, T.; Baldo, M. A. External Quantum Efficiency Above 100% in a Singlet-Exciton-Fission−Based Organic Photovoltaic Cell. *Science* **2013**, *340*, 334−337.

(4) Xiong, H.; Zhou, K.; Yan, Y.; Miller, J. B.; Siegwart, D. J. Tumor-Activated Water-Soluble Photosensitizers for Near-Infrared Photodynamic Cancer Therapy. *ACS Appl. Mater. Interfaces* **2018**, *10*, 16335−16343.

(5) Li, X.; Kolemen, S.; Yoon, J.; Akkaya, E. U. Activatable Photosensitizers: Agents for Selective Photodynamic Therapy. *Adv. Funct. Mater.* **2017**, *27*, 1604053.

(6) Cló, E.; Snyder, J. W.; Ogilby, P. R.; Gothelf, K. V. Control and Selectivity of Photosensitized Singlet Oxygen Production: Challenges in Complex Biological Systems. *ChemBioChem* **2007**, *8*, 475−481.

(7) Kamkaew, A.; Lim, S. H.; Lee, H. B.; Kiew, L. V.; Chung, L. Y.; Burgess, K. BODIPY dyes in photodynamic therapy. *Chem. Soc. Rev.* **2013**, *42*, 77−88.

(8) Awuah, S. G.; You, Y. Boron dipyrromethene (BODIPY)-based photosensitizers for photodynamic therapy. *RSC Adv.* **2012**, *2*, 11169−11183.
(9) Weijer, R.; Broekgaarden, M.; Kos, M.; van Vught, R.; Rauws, E. A. J.; Breukink, E.; van Gulik, T. M.; Storm, G.; Heger, M. Enhancing photodynamic therapy of refractory solid cancers: Combining second-generation photosensitizers with multi-targeted liposomal delivery. *J. Photochem. Photobiol. C: Photochem. Rev.* **2015**, *23*, 103−131.
(10) Pushalkar, S.; Ghosh, G.; Xu, Q.; Liu, Y.; Ghogare, A. A.; Atem, C.; Greer, A.; Saxena, D.; Lyons, A. M. Superhydrophobic Photosensitizers: Airborne$^1O_2$Killing of an in Vitro Oral Biofilm at the Plastron Interface. *ACS Appl. Mater. Interfaces* **2018**, *10*, 25819−25829.
(11) Liu, Q.; Yang, T.; Feng, W.; Li, F. Blue-Emissive Upconversion Nanoparticles for Low-Power-Excited Bioimaging in Vivo. *J. Am. Chem. Soc.* **2012**, *134*, 5390−5397.
(12) Zhang, K. Y.; Zhang, T.; Wei, H.; Wu, Q.; Liu, S.; Zhao, Q.; Huang, W. Phosphorescent iridium(III) complexes capable of imaging and distinguishing between exogenous and endogenous analytes in living cells. *Chem. Sci.* **2018**, *9*, 7236−7240.
(13) Wu, Y.; Zhen, Y.; Wang, Z.; Fu, H. Donor-Linked Di(perylene bisimide)s: Arrays Exhibiting Fast Electron Transfer for Photosynthesis Mimics. *J. Phys. Chem. A* **2013**, *117*, 1712−1720.
(14) Wang, Z.; Zhao, J.; Di Donato, M.; Mazzone, G. Increasing the anti-Stokes shift in TTA upconversion with photosensitizers showing red-shifted spin-allowed charge transfer absorption but a non-compromised triplet state energy level. *Chem. Commun.* **2019**, *55*, 1510−1513.
(15) Pun, A. B.; Sanders, S. N.; Sfeir, M. Y.; Campos, L. M.; Congreve, D. N. Annihilator dimers enhance triplet fusion upconversion. *Chem. Sci.* **2019**, *10*, 3969−3975.
(16) Liu, H.; Yan, X.; Shen, L.; Tang, Z.; Liu, S.; Li, X. Color-tunable upconversion emission from a twisted intramolecular charge-transfer state of anthracene dimers via triplet−triplet annihilation. *Mater. Horiz.* **2019**, *6*, 990−995.
(17) Mahmood, Z.; Zhao, J. Thiol-Activatable Triplet−Triplet Annihilation Upconversion with Maleimide-Perylene as the Caged Triplet Acceptor/Emitter. *J. Org. Chem.* **2016**, *81*, 587−594.
(18) Monguzzi, A.; Tubino, R.; Hoseinkhani, S.; Campione, M.; Meinardi, F. Low power, non-coherent sensitized photon up-conversion: modelling and perspectives. *Phys. Chem. Chem. Phys.* **2012**, *14*, 4322−4332.
(19) Zhou, J.; Liu, Q.; Feng, W.; Sun, Y.; Li, F. Upconversion Luminescent Materials: Advances and Applications. *Chem. Rev.* **2015**, *115*, 395−465.
(20) Simon, Y. C.; Weder, C. Low-power photon upconversion through triplet-triplet annihilation in polymers. *J. Mater. Chem.* **2012**, *22*, 20817−20830.
(21) Singh-Rachford, T. N.; Castellano, F. N. Photon upconversion based on sensitized triplet−triplet annihilation. *Coord. Chem. Rev.* **2010**, *254*, 2560−2573.
(22) Wu, X.; Zhu, W. Stability enhancement of fluorophores for lighting up practical application in bioimaging. *Chem. Soc. Rev.* **2015**, *44*, 4179−4184.
(23) Lu, H.; Mack, J.; Yang, Y.; Shen, Z. Structural modification strategies for the rational design of red/NIR region BODIPYs. *Chem. Soc. Rev.* **2014**, *43*, 4778−4823.
(24) Buck, J. T.; Boudreau, A. M.; DeCarmine, A.; Wilson, R. W.; Hampsey, J.; Mani, T. Spin-Allowed Transitions Control the Formation of Triplet Excited States in Orthogonal Donor-Acceptor Dyads. *Chem* **2019**, *5*, 138−155.
(25) Filatov, M. A.; Karuthedath, S.; Polestshuk, P. M.; Savoie, H.; Flanagan, K. J.; Sy, C.; Sitte, E.; Telitchko, M.; Laquai, F.; Boyle, R. W.; et al. Generation of Triplet Excited States via Photoinduced Electron Transfer in meso-anthra-BODIPY: Fluorogenic Response toward Singlet Oxygen in Solution and in Vitro. *J. Am. Chem. Soc.* **2017**, *139*, 6282−6285.
(26) Ziessel, R.; Allen, B. D.; Rewinska, D. B.; Harriman, A. Selective Triplet-State Formation during Charge Recombination in a Fullerene/Bodipy Molecular Dyad (Bodipy = Borondipyrromethene). *Chem. − Eur. J.* **2009**, *15*, 7382−7393.
(27) Amin, A. N.; El-Khouly, M. E.; Subbaiyan, N. K.; Zandler, M. E.; Fukuzumi, S.; D'Souza, F. A novel BF_2-chelated azadipyrromethene−fullerene dyad: synthesis, electrochemistry and photodynamics. *Chem. Commun.* **2012**, *48*, 206−208.
(28) Guo, S.; Xu, L.; Xu, K.; Zhao, J.; Küçüköz, B.; Karatay, A.; Yaglioglu, H. G.; Hayvali, M.; Elmali, A. Bodipy−C_{60}triple hydrogen bonding assemblies as heavy atom-free triplet photosensitizers: preparation and study of the singlet/triplet energy transfer. *Chem. Sci.* **2015**, *6*, 3724−3737.
(29) Wu, W.; Guo, H.; Wu, W.; Ji, S.; Zhao, J. Organic Triplet Sensitizer Library Derived from a Single Chromophore (BODIPY) with Long-Lived Triplet Excited State for Triplet−Triplet Annihilation Based Upconversion. *J. Org. Chem.* **2011**, *76*, 7056−7064.
(30) Yogo, T.; Urano, Y.; Ishitsuka, Y.; Maniwa, F.; Nagano, T. Highly Efficient and Photostable Photosensitizer Based on BODIPY Chromophore. *J. Am. Chem. Soc.* **2005**, *127*, 12162−12163.
(31) Adarsh, N.; Avirah, R. R.; Ramaiah, D. Tuning Photosensitized Singlet Oxygen Generation Efficiency of Novel Aza-BODIPY Dyes. *Org. Lett.* **2010**, *12*, 5720−5723.
(32) Sabatini, R. P.; McCormick, T. M.; Lazarides, T.; Wilson, K. C.; Eisenberg, R.; McCamant, D. W. Intersystem Crossing in Halogenated Bodipy Chromophores Used for Solar Hydrogen Production. *J. Phys. Chem. Lett.* **2011**, *2*, 223−227.
(33) Castellano, F. N.; Pomestchenko, I. E.; Shikhova, E.; Hua, F.; Muro, M. L.; Rajapakse, N. Photophysics in bipyridyl and terpyridyl platinum(II) acetylides. *Coord. Chem. Rev.* **2006**, *250*, 1819−1828.
(34) You, Y.; Nam, W. Photofunctional triplet excited states of cyclometalated Ir(III) complexes: beyond electroluminescence. *Chem. Soc. Rev.* **2012**, *41*, 7061−7084.
(35) Chi, Y.; Chou, P.-T. Contemporary progresses on neutral, highly emissive Os(II) and Ru(II) complexes. *Chem. Soc. Rev.* **2007**, *36*, 1421−1431.
(36) Rajagopal, S. K.; Mallia, A. R.; Hariharan, M. Enhanced intersystem crossing in carbonylpyrenes. *Phys.Chem. Chem. Phys.* **2017**, *19*, 28225−28231.
(37) Pang, W.; Zhang, X.-F.; Zhou, J.; Yu, C.; Hao, E.; Jiao, L. Modulating the singlet oxygen generation property of meso−β directly linked BODIPY dimers. *Chem. Commun.* **2012**, *48*, 5437−5439.
(38) Ventura, B.; Marconi, G.; Bröring, M.; Krüger, R.; Flamigni, L. Bis(BF_2)-2,2′-bidipyrrins, a class of BODIPY dyes with new spectroscopic and photophysical properties. *New J. Chem.* **2009**, *33*, 428−438.
(39) Bröring, M.; Krüger, R.; Link, S.; Kleeberg, C.; Köhler, S.; Xie, X.; Ventura, B.; Flamigni, L. Bis(BF_2)-2,2′-Bidipyrrins (BisBODIPYs): Highly Fluorescent BODIPY Dimers with Large Stokes Shifts. *Chem. − Eur. J.* **2008**, *14*, 2976−2983.
(40) Huang, L.; Cui, X.; Therrien, B.; Zhao, J. Energy-Funneling-Based Broadband Visible-Light-Absorbing Bodipy−C_{60} Triads and Tetrads as Dual Functional Heavy-Atom-Free Organic Triplet Photosensitizers for Photocatalytic Organic Reactions. *Chem. − Eur. J.* **2013**, *19*, 17472−17482.
(41) Wu, W.; Zhao, J.; Sun, J.; Guo, S. Light-Harvesting Fullerene Dyads as Organic Triplet Photosensitizers for Triplet−Triplet Annihilation Upconversions. *J. Org. Chem.* **2012**, *77*, 5305−5312.
(42) Huang, L.; Yu, X.; Wu, W.; Zhao, J. Styryl Bodipy-C_{60} Dyads as Efficient Heavy-Atom-Free Organic Triplet Photosensitizers. *Org. Lett.* **2012**, *14*, 2594−2597.
(43) Huang, D.; Zhao, J.; Wu, W.; Yi, X.; Yang, P.; Ma, J. Visible-Light-Harvesting Triphenylamine Ethynyl C_{60}-BODIPY Dyads as Heavy-Atom-Free Organic Triplet Photosensitizers for Triplet-Triplet Annihilation Upconversion. *Asian J. Org. Chem.* **2012**, *1*, 264−273.
(44) Zhao, J.; Wu, W.; Sun, J.; Guo, S. Triplet photosensitizers: from molecular design to applications. *Chem. Soc. Rev.* **2013**, *42*, 5323−5351.

https://dx.doi.org/10.1021/acs.jpcc.9b11687
J. Phys. Chem. C XXXX, XXX, XXX−XXX

(45) Zhao, J.; Xu, K.; Yang, W.; Wang, Z.; Zhong, F. The triplet excited state of Bodipy: formation, modulation and application. *Chem. Soc. Rev.* **2015**, *44*, 8904−8939.
(46) Golden, J. H.; Estergreen, L.; Porter, T.; Tadle, A. C.; Sylvinson, M. R. D.; Facendola, J. W.; Kubiak, C. P.; Bradforth, S. E.; Thompson, M. E. Symmetry-Breaking Charge Transfer in Boron Dipyridylmethene (DIPYR) Dimers. *ACS Appl. Energy Mater.* **2018**, *1*, 1083−1095.
(47) Das, S.; Thornbury, W. G.; Bartynski, A. N.; Thompson, M. E.; Bradforth, S. E. Manipulating Triplet Yield through Control of Symmetry-Breaking Charge Transfer. *J. Phys. Chem. Lett.* **2018**, *9*, 3264−3270.
(48) Wang, Z.; Zhao, J.; Barbon, A.; Toffoletti, A.; Liu, Y.; An, Y.; Xu, L.; Karatay, A.; Yaglioglu, H. G.; Yildiz, E. A.; Hayvali, M. Radical-Enhanced Intersystem Crossing in New Bodipy Derivatives and Application for Efficient Triplet−Triplet Annihilation Upconversion. *J. Am. Chem. Soc.* **2017**, *139*, 7831−7842.
(49) Wang, Z.; Gao, Y.; Hussain, M.; Kundu, S.; Rane, V.; Hayvali, M.; Yildiz, E. A.; Zhao, J.; Yaglioglu, H. G.; Das, R.; et al. Efficient Radical-Enhanced Intersystem Crossing in an NDI-TEMPO Dyad: Photophysics, Electron Spin Polarization, and Application in Photodynamic Therapy. *Chem. − Eur. J.* **2018**, *24*, 18663−18675.
(50) Dance, Z. E. X.; Mi, Q.; McCamant, D. W.; Ahrens, M. J.; Ratner, M. A.; Wasielewski, M. R. Time-Resolved EPR Studies of Photogenerated Radical Ion Pairs Separated by p-Phenylene Oligomers and of Triplet States Resulting from Charge Recombination. *J. Phys. Chem. B* **2006**, *110*, 25163−25173.
(51) Colvin, M. T.; Ricks, A. B.; Scott, A. M.; Co, D. T.; Wasielewski, M. R. Intersystem Crossing Involving Strongly Spin Exchange-Coupled Radical Ion Pairs in Donor−bridge−Acceptor Molecules. *J. Phys. Chem. A* **2012**, *116*, 1923−1930.
(52) Verhoeven, J. W.; van Ramesdonk, H. J.; Groeneveld, M. M.; Benniston, A. C.; Harriman, A. Long-Lived Charge-Transfer States in Compact Donor−Acceptor Dyads. *ChemPhysChem* **2005**, *6*, 2251−2260.
(53) Weiss, E. A.; Ratner, M. A.; Wasielewski, M. R. Direct Measurement of Singlet−Triplet Splitting within Rodlike Photogenerated Radical Ion Pairs Using Magnetic Field Effects: Estimation of the Electronic Coupling for Charge Recombination. *J. Phys. Chem. A* **2003**, *107*, 3639−3647.
(54) Verhoeven, J. W. On the role of spin correlation in the formation, decay, and detection of long-lived, intramolecular charge-transfer states. *J. Photochem. Photobiol. C: Photochem. Rev* **2006**, *7*, 40−60.
(55) Epelde-Elezcano, N.; Palao, E.; Manzano, H.; Prieto-Castañeda, A.; Agarrabeitia, A. R.; Tabero, A.; Villanueva, A.; de la Moya, S.; López-Arbeloa, Í.; Martínez-Martínez, V.; Ortiz, M. J. Rational Design of Advanced Photosensitizers Based on Orthogonal BODIPY Dimers to Finely Modulate Singlet Oxygen Generation. *Chem. −Eur. J.* **2017**, *23*, 4837−4848.
(56) van Willigen, H.; Jones, G.; Farahat, M. S. Time-Resolved EPR Study of Photoexcited Triplet-State Formation in Electron-Donor-Substituted Acridinium Ions. *J. Phys. Chem.* **1996**, *100*, 3312−3316.
(57) Dance, Z. E. X.; Mickley, S. M.; Wilson, T. M.; Ricks, A. B.; Scott, A. M.; Ratner, M. A.; Wasielewski, M. R. Intersystem Crossing Mediated by Photoinduced Intramolecular Charge Transfer: Julolidine−Anthracene Molecules with Perpendicular π Systems. *J. Phys. Chem. A* **2008**, *112*, 4194−4201.
(58) Zhao, Y.; Duan, R.; Zhao, J.; Li, C. Spin−orbit charge transfer intersystem crossing in perylenemonoimide−phenothiazine compact electron donor−acceptor dyads. *Chem. Commun.* **2018**, *54*, 12329−12332.
(59) Chen, K.; Yang, W.; Wang, Z.; Iagatti, A.; Bussotti, L.; Foggi, P.; Ji, W.; Zhao, J.; Di Donato, M. Triplet Excited State of BODIPY Accessed by Charge Recombination and Its Application in Triplet−Triplet Annihilation Upconversion. *J. Phys. Chem. A* **2017**, *121*, 7550−7564.
(60) Hou, Y.; Biskup, T.; Rein, S.; Wang, Z.; Bussotti, L.; Russo, N.; Foggi, P.; Zhao, J.; Di Donato, M.; Mazzone, G.; et al. Spin−Orbit Charge Recombination Intersystem Crossing in Phenothiazine−Anthracene Compact Dyads: Effect of Molecular Conformation on Electronic Coupling, Electronic Transitions, and Electron Spin Polarizations of the Triplet States. *J. Phys. Chem. C* **2018**, *122*, 27850−27865.
(61) Wang, Z.; Zhao, J. Bodipy−Anthracene Dyads as Triplet Photosensitizers: Effect of Chromophore Orientation on Triplet-State Formation Efficiency and Application in Triplet−Triplet Annihilation Upconversion. *Org. Lett.* **2017**, *19*, 4492−4495.
(62) Wang, Z.; Sukhanov, A. A.; Toffoletti, A.; Sadiq, F.; Zhao, J.; Barbon, A.; Voronkova, V. K.; Dick, B. Insights into the Efficient Intersystem Crossing of Bodipy-Anthracene Compact Dyads with Steady-State and Time-Resolved Optical/Magnetic Spectroscopies and Observation of the Delayed Fluorescence. *J. Phys. Chem. C* **2019**, *123*, 265−274.
(63) Zhong, Y.-W.; Gong, Z.-L.; Shao, J.-Y.; Yao, J. Electronic coupling in cyclometalated ruthenium complexes. *Coord. Chem. Rev.* **2016**, *312*, 22−40.
(64) Zhang, X.-F.; Yang, X. Photosensitizer That Selectively Generates Singlet Oxygen in Nonpolar Environments: Photophysical Mechanism and Efficiency for a Covalent BODIPY Dimer. *J. Phys. Chem. B* **2013**, *117*, 9050−9055.
(65) Sasaki, S.; Hattori, K.; Igawa, K.; Konishi, G.-i. Directional Control of π-Conjugation Enabled by Distortion of the Donor Plane in Diarylaminoanthracenes: A Photophysical Study. *J. Phys. Chem. A* **2015**, *119*, 4898−4906.
(66) D'Souza, F.; Chitta, R.; Ohkubo, K.; Tasior, M.; Subbaiyan, N. K.; Zandler, M. E.; Rogacki, M. K.; Gryko, D. T.; Fukuzumi, S. Corrole−Fullerene Dyads: Formation of Long-Lived Charge-Separated States in Nonpolar Solvents. *J. Am. Chem. Soc.* **2008**, *130*, 14263−14272.
(67) Zhang, X.-F.; Wang, J. Morpholine-Phthalocyanine (Donor−Acceptor) Construct: Photoinduced Intramolecular Electron Transfer and Triplet Formation from its Charge Separation State. *J. Phys. Chem. A* **2011**, *115*, 8597−8603.
(68) Mahmood, Z.; Zhao, J. The unquenched triplet excited state of the fluorescent OFF/ON Bodipy-derived molecular probe based on photo-induced electron transfer. *Photochem. Photobiol. Sci.* **2016**, *15*, 1358−1365.
(69) Zhao, Y.; Li, X.; Wang, Z.; Yang, W.; Chen, K.; Zhao, J.; Gurzadyan, G. G. Precise Control of the Electronic Coupling Magnitude between the Electron Donor and Acceptor in Perylenebisimide Derivatives via Conformation Restriction and Its Effect on Photophysical Properties. *J. Phys. Chem. C* **2018**, *122*, 3756−3772.
(70) Zhang, X.-F.; Yang, X. Singlet Oxygen Generation and Triplet Excited-State Spectra of Brominated BODIPY. *J. Phys. Chem. B* **2013**, *117*, 5533−5539.
(71) Filatov, M. A.; Karuthedath, S.; Polestshuk, P. M.; Callaghan, S.; Flanagan, K. J.; Telitchko, M.; Wiesner, T.; Laquai, F.; Senge, M. O. Control of triplet state generation in heavy atom-free BODIPY−anthracene dyads by media polarity and structural factors. *Phys. Chem. Chem. Phys.* **2018**, *20*, 8016−8031.
(72) Niladari Raju, M. V.; Mohanty, M. E.; Bangal, P. R.; Vaidya, J. R. Synthesis and Ultrafast Dynamics of a Donor−Acceptor−Donor Molecule Having Optoelectronic Properties. *J. Phys. Chem. C* **2015**, *119*, 8563−8575.
(73) Tao, Y.; Yuan, K.; Chen, T.; Xu, P.; Li, H.; Chen, R.; Zheng, C.; Zhang, L.; Huang, W. Thermally Activated Delayed Fluorescence Materials Towards the Breakthrough of Organoelectronics. *Adv. Mater.* **2014**, *26*, 7931−7958.
(74) Im, Y.; Byun, S. Y.; Kim, J. H.; Lee, D. R.; Oh, C. S.; Yook, K. S.; Lee, J. Y. Recent Progress in High-Efficiency Blue-Light-Emitting Materials for Organic Light-Emitting Diodes. *Adv. Funct. Mater.* **2017**, *27*, 1603007.
(75) Ye, H.; Kim, D. H.; Chen, X.; Sandanayaka, A. S. D.; Kim, J. U.; Zaborova, E.; Canard, G.; Tsuchiya, Y.; Choi, E. Y.; Wu, J. W.; et al. Near-Infrared Electroluminescence and Low Threshold Amplified

https://dx.doi.org/10.1021/acs.jpcc.9b11687
J. Phys. Chem. C XXXX, XXX, XXX−XXX

1109 Spontaneous Emission above 800 nm from a Thermally Activated
1110 Delayed Fluorescent Emitter. *Chem. Mater.* **2018**, *30*, 6702−6710.
1111 (76) Serevičius, T.; Komskis, R.; Adomėnas, P.; Adomėnienė, O.;
1112 Kreiza, G.; Jankauskas, V.; Kazlauskas, K.; Miasojedovas, A.; Jankus,
1113 V.; Monkman, A.; et al. Triplet−Triplet Annihilation in 9,10-
1114 Diphenylanthracene Derivatives: The Role of Intersystem Crossing
1115 and Exciton Diffusion. *J. Phys. Chem. C* **2017**, *121*, 8515−8524.
1116 (77) van Stokkum, I. H. M.; Larsen, D. S.; van Grondelle, R. Global
1117 and target analysis of time-resolved spectra. *BBA - Bioenergetics* **2004**,
1118 *1657*, 82−104.
1119 (78) Henry, E. R.; Hofrichter, J. [8] Singular value decomposition:
1120 Application to analysis of experimental data. *Methods in Enzymol.*
1121 1992, *210*, 129−192, DOI: 10.1016/0076-6879(92)10010-B.
1122 (79) Snellenburg, J. J.; Laptenok, S.; Seger, R.; Mullen, K. M.; Van
1123 Stokkum, I. H. M. Glotaran: A Java-based graphical user interface for
1124 the R package TIMP. *J. Stat. Software* **2012**, *49*, 1−22.

https://dx.doi.org/10.1021/acs.jpcc.9b11687
J. Phys. Chem. C XXXX, XXX, XXX−XXX